arXiv:0909.4311v1 [astro-ph.CO] 24 Sep 2009

POLARIZATION OF THE WMAP POINT SOURCES

M. López-Caniego
Instituto de Física de Cantabria (CSIC-UC), Santander, Spain 39005 and
Astrophysics Group, Cavendish Laboratory, J.J. Thomson Avenue, Cambridge, United Kingdom CB3 0E1

M. Massardi
INAF-Ossevatorio Astronomico di Padova, Padova, Italy 35122

J. González-Nuevo
SISSA-I.S.A.S, Trieste, Italy 34014

L. Lanz
Instituto de Física de Cantabria (CSIC-UC), Santander, Spain 39005 and
Departamento de Física Moderna, Universidad de Cantabria, Santander, Spain 39005

D. Herranz
Instituto de Física de Cantabria (CSIC-UC), Santander, Spain 39005

G. De Zotti
INAF-Ossevatorio Astronomico di Padova, Padova, Italy 35122 and
SISSA-I.S.A.S, Trieste, Italy 34014

J.L. Sanz
Instituto de Física de Cantabria (CSIC-UC), Santander, Spain 39005

and

F. Argüeso
Departamento de Matemáticas, Universidad de Oviedo, Oviedo, Spain 33007
Draft version September 24, 2009

ABSTRACT

The detection of polarized sources in the WMAP 5-year data is a very difficult task. The maps are dominated by instrumental noise and only a handful of sources show up as clear peaks in the Q and U maps. Optimal linear filters applied at the position of known bright sources detect with a high level of significance a polarized flux P from many more sources, but estimates of P are liable to biases. Using a new technique, named the *filtered fusion technique*, we have detected in polarization, with a significance level greater than 99.99% in at least one WMAP channel, 22 objects, 5 of which, however, do not have a plausible low radio frequency counterpart and are therefore doubtful. Estimated polarized fluxes $P < 400\,\mathrm{mJy}$ at 23 GHz were found to be severely affected by the Eddington bias. The corresponding polarized flux limit for Planck/LFI at 30 GHz, obtained via realistic simulations, is 300 mJy. We have also obtained statistical estimates of, or upper limits to the mean polarization degrees of bright WMAP sources at 23, 33, 41, and 61 GHz, finding that they are of a few percent.

Subject headings: filters: filters; point sources: catalogues, identifications, polarization

1. INTRODUCTION

Studies of Cosmic Microwave Background (CMB) anisotropy are a top scientific priority since they address the deepest questions about origin, structure, and equation of state of the Universe. Given the sensitivity of current detectors, the main constraint on our ability to accurately map CMB anisotropies is set by foreground emissions. While these signals have contaminated, but not dominated, temperature maps, they are a far bigger problem for CMB polarization. Also, fighting this

Electronic address: caniego@ifca.unican.es

contamination is more difficult because we know much less about polarization than we do about total intensity emission. The Task Force on CMB Research (Bock et al. 2006) indeed regards a better characterization of polarized foregrounds as "a key milestone" in their proposed roadmap.

Extragalactic radio sources are the main CMB contaminant on angular scales below $0.5°$ at frequencies of up to $\simeq 100$ GHz (Tucci et al. 2005). Observational studies of high-frequency polarization are still scanty and mostly dealing with sources selected at lower frequencies as shown in Ricci et al. (2004) and in the references in Table 3 of Tucci et al. (2004). The blind Australia

Telescope 20 GHz (AT20G) survey of the Southern sky includes polarization measurements at 20, 8.6 and 4.8 GHz; data have been published for the bright source sample (Massardi et al. 2008; Burke-Spolaor et al. 2009).

The WMAP survey has yielded the first all-sky total intensity and polarization surveys at frequencies from 23 to 94 GHz. The analysis of 5-yr data (Wright et al. 2009) showed that, in general, the WMAP detected point sources are not strongly polarized. Only 5 (Fornax A, Pictor A, 3C 273, Virgo A, and 3C 279) were found to have polarization degrees greater than 4% in two or more bands. In this paper we plan to complement and improve on their analysis in two basic respects. On one side, we apply a non-blind approach to source detection in polarization, exploiting the knowledge of positions of the brightest sources in total intensity, and a new detection technique, called the filtered fusion technique (Argüeso et al. 2009), taking into account the real beam profiles. On the other side, we check the reliability of our estimates of polarized flux densities by comparison with the very high signal-to-noise AT20G BSS (Massardi et al. 2008), Ricci et al. (2004), and high frequency VLA calibrator measurements, and by means of numerical simulations. We also present an estimate of the mean polarization of sources in a total flux density limited sample.

The polarization is measured by the Stokes parameters $\hat{Q}$, $\hat{U}$ and $\hat{V}$, and the polarized intensity is $\hat{P} = \sqrt{\hat{Q}^2 + \hat{U}^2 + \hat{V}^2}$, see Kamionkowski, Kosowsky & Stebbins (1997) for further details. If we consider linear polarization, $\hat{V} = 0$, which is justified by the fact that extragalactic radio sources have very low levels of circular polarisation (Homan, Attridge & Wardle 2001), we have to combine $\hat{Q}$ and $\hat{U}$ maps in an appropriate way to avoid biasing the estimates of $\hat{P}$. Furthermore, the polarized signal is just a small fraction of the total intensity signal, of the order of a few percent, which makes it hard to detect. In the case of WMAP polarization maps, only a couple of sources can be seen by eye. This situation may exacerbate the problems with the Eddington (1913) bias (sources are more easily detected if they happen to lie on top of positive fluctuations, so that, on average, their fluxes are overestimated), highlighted by Massardi et al. (2009) for WMAP sources close to the detection limit in total flux. This issue will be further investigated.

The outline of this paper is as follows. In § 2 we describe our method and the sample of WMAP sources, bright in total flux, to which it was applied to estimate their polarized flux. In § 3 we discuss the results, also in comparison with high signal-to-noise ground based measurements at similar frequencies. Finally, in § 4, we summarize our main conclusions.

2. METHODOLOGY

2.1. *The Input Catalog*

We have carried out a systematic investigation of the polarized flux of the 516 sources detected at $\geq 5\sigma$ by Massardi et al. (2009) in the 5-yr WMAP temperature maps, and listed in the NEWPS_5yr_5s catalogue[1]. 484

[1] http://max.ifca.unican.es/caniego/NEWPS

of these sources have a clear identification in low frequency catalogues (including 27 Galactic objects); the 5 objects detected in polarization by Wright et al. (2009) belong to this group. The remaining 32 candidate sources do not have plausible counterparts in all-sky low radio frequency surveys and may therefore be just high peaks in the highly non-Gaussian distribution of the other components present in the maps. If they are all spurious, the reliability of the sample is 94% and its completeness is of 91% above 1 Jy.

Since one of our goals is to define a sample as large as possible of potential calibrators for CMB polarization experiments, we have added 3 extended sources (Cygnus A, Taurus A, Cas A), not included in the catalog because they lie in very noisy regions, close to the Galactic equator, but known to be very bright and significantly polarized. The full sample (Input Catalog) is thus made of 519 sources.

2.2. *Filtered Fusion*

Methods to extract astrophysical foregrounds from multi-frequency CMB maps frequently exploit the prior knowledge of their frequency dependence. This approach however does not work well for radio sources because of the broad variety of their spectral properties in the relevant frequency range (Massardi et al. 2008; Sadler et al. 2008). On the other hand, with few exceptions, extragalactic radio sources look point-like when observed with the beams used by CMB experiments, and therefore have, in the maps, the shape of the effective angular response function of the instrument. In the literature one can find several methods exploiting this property and using linear filters to detect point sources. The standard matched filter approach has been used for years (Nailong 1992; Vikhlinin et al. 1995; Malik & Subramanian 1997; Tegmark & de Oliveira-Costa 1998; Sanz, Herranz & Martínez-Gónzalez 2001; Herranz et al. 2002; Stewart 2006). More recently, a multi-frequency approach based on matched filters has been elaborated (Herranz et al. 2009; Herranz & Sanz 2008). An approach based on optimal wavelets (Vielva et al. 2001, 2003; Barnard et al. 2004; Sanz et al. 2006; González-Nuevo et al. 2006) was successfully applied to WMAP maps (López-Caniego et al. 2007; Massardi et al. 2009) as well as to realistic simulations of Planck maps (López-Caniego et al. 2006; Leach et al. 2008). Moreover, filters based on the Neyman-Pearson approach, using the distribution of maxima, have been proposed (López-Caniego et al. 2005a,b) and a Bayesian approach has been developed (Hobson & McLachlan 2003; Feroz & Hobson 2008; Carvalho, Rocha, & Hobson 2009).

In this work, following Argüeso et al. (2009), we use the same matched filter over Q and U images. The matched filter is a circularly-symmetric filter, $\Psi(x; R, b)$, such that the filtered map, $w(R, b)$ satisfies the following two conditions: (1) $\langle w(R_0, 0) \rangle = s(0) \equiv A$, i.e. $w(R, 0)$ is an *unbiased* estimator of the flux density of the source; (2) the variance of $w(R, b)$ has a minimum on the scale R_0, i.e. it is an *efficient* estimator. In Fourier space the matched filter writes as:

$$\psi_{MF} = \frac{1}{a}\frac{\tau(q)}{\Delta(q)}, \quad a = 2\pi \int dq\, q \frac{\tau^2(q)}{\Delta(q)}, \qquad (1)$$
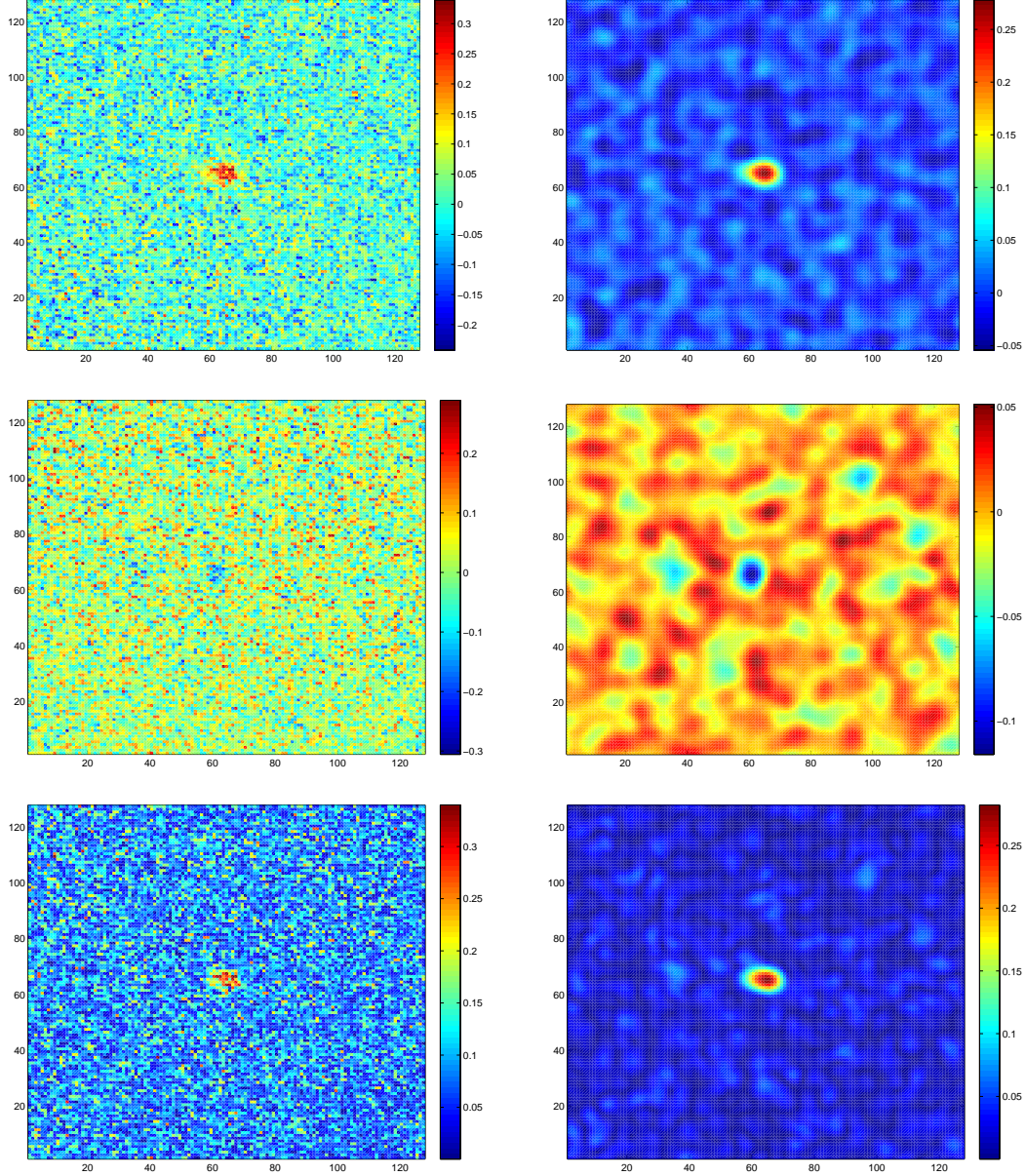
FIG. 1.— Polarization maps at 23 GHz centered on the position of Fornax A (no. 74 in the NEWPS_5yr_5s catalogue). The upper left-and right-hand panels show, respectively, the maps of $\hat{Q}$ and Q before and after filtering with the matched filter, while the middle panels show the analogous $\hat{U}$ and U maps. The lower panels show, for the same source, the maps of $\hat{P} = \sqrt{\hat{Q}^2 + \hat{U}^2}$ (left) and $P = \sqrt{Q^2 + U^2}$ (right).

where $\Delta(q)$ is the power spectrum of the background and $\tau(q)$ is Fourier transform of the source profile (equal to the beam profile for point sources).

Since, in this application, each patch is centered on the position of a source detected in total intensity, we describe the source as

$$s(\vec{x}) = A\tau(\vec{x}), \qquad (2)$$

where A is its unknown polarized flux density and $\tau(\vec{x})$ is its *profile*. We assume circular symmetry, so that $\tau(\vec{x}) = \tau(x)$, $x = |\vec{x}|$. For point sources the profile is equal to the beam response function of the detector. The WMAP beams are not Gaussian and we use the real symmetrized

radial beam profiles for the different WMAP channels to construct our filters.

The matched filter gives directly the maximum amplification of the source and yields the best linear estimation of the flux. As extensively discussed in the literature, it is a very powerful tool to detect point sources, but it has to be used with care because its performance may degrade rapidly if it is not properly implemented. In particular, the power spectrum $\Delta(q)$ of the image has to be obtained directly from the data.

The WMAP team has used a matched filter that operates on the sphere and takes into account the non-Gaussian profile of the beam. It is described by eq. (1),

replacing the flat limit quantities $\tau(q)$ and $\Delta(q)$ with their harmonic equivalents b_ℓ and C_ℓ. As pointed out by López-Caniego et al. (2006), the use of the C_ℓ's computed from all-sky maps to construct a global matched filter that operates on the sphere is a reasonable first approach, but we think that it can be improved by operating locally.

We have followed the scheme named *filtered fusion* by its authors (Argüeso et al. 2009). For each object in the input catalog, and for each WMAP frequency between 23 and 61 GHz, we have projected two patches (one for Q and one for U), each of 14.65×14.65 square degrees, centered on the source position. We have left aside the 94 GHz channel because of the normalization problems discussed by López-Caniego et al. (2007) and González-Nuevo et al. (2008). Each patch is made of 128×128 6.87 arcmin pixels (HealPix Nside = 512, Górski et al. (2005)). The projection has been done using the CPACK library[2]. Then, each pair of patches has been filtered using a matched filter exploiting the power spectrum determined within each patch. After filtering, the Q^2 and U^2 are added together and the square root of the resulting image has been calculated. The noise bias can be removed by subtracting from Q^2 and U^2 the corresponding noise contribution $\sigma_{\hat{Q}}^2$ and $\sigma_{\hat{U}}^2$. This correction turns out to be negligible. In this way we have obtained a map of the polarized intensity P within each patch. This approach differs from the usual one, where a $\hat{P}$ map is constructed adding together the unfiltered $\hat{Q}^2$ and $\hat{U}^2$ maps, and taking the square root of the resulting map (see Fig. 1).

We have then looked for the brightest maximum inside a circle centered on the center of each patch and covering the area of the WMAP beam. Next, we estimated the noise level of the patch and the significance of the possible detection. Finally, we constructed catalogues containing all sources whose polarized flux P was detected above a chosen significance level.

The reason why we need to use the significance of the detection instead of the usual signal-to-noise ratio is that the noise does not obey a Gaussian distribution but a Rayleigh distribution, since we are dealing with maps that have been squared. The significance was derived from the distribution of the values of P for the pixels within the patch. An example of such distribution is in Fig. 2.

2.3. *Flux and error estimation*

The polarized flux densities and their errors were estimated in a way similar to that applied for total intensity (Massardi et al. 2009). Point sources appear in the image with a profile identical to the beam profile. For example, if the beams were Gaussian, the source flux could be obtained multiplying the flux in the brightest pixel by the ratio between the beam and the pixel area, $2\pi(R_s)^2/L_p^2$, where $R_s = \mathrm{FWHM}/(2\sqrt{2\log 2})$ and L_p is the pixel side.

In our case the beams are not Gaussian and we need to calculate this relationship integrating over the real symmetrized beam profile for each channel. In doing that we have to take into account that we work with HEALPix pixelization (Górski et al. 2005) at Nside=512. Although
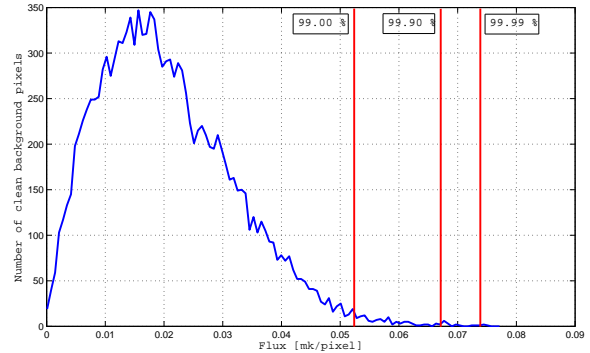
[2] http://astro.ic.ac.uk/mortlock/cpack/

Fig. 2.— Histogram showing the distribution of the polarized flux $P = \sqrt{(Q^2 + U^2)}$ (in mK per pixel) obtained from a filtered WMAP 23 GHz patch of $\hat{Q}$ and $\hat{U}$ centered on the position of Fornax A (14.65 square degree patch and 128x128 pixels). This histogram has been produced with the values of ~ 13500 pixels, excluding the flagged ones (see Fig. 3). The vertical lines correspond to the values of P exceeding those of 99.0%, 99.9%, and 99.99% of the pixels. In other words, measured values of P at these levels have, respectively, 99.0%, 99.9%, and 99.99% probability of *not* being due to noise spikes. Note that the polarized flux of a source is obtained multiplying the flux in the brightest pixel by the ratio between the beam and the pixel area (see § 2.3).

the image is centered at the position of the source, after the projection to the flat patch the object does not always lie in the central pixel, but may end up in an adjacent one. Thus, to estimate its flux we make reference not to the intensity in the central pixel but to that of the brightest pixel close to the center of the *filtered* image within an area equal to that of the beam. As discussed in § 3.3 of López-Caniego et al. (2007), this method for flux estimation through linear filtering is almost optimal in many circumstances.

Note that the method adopted here to estimate the flux differs from the one used by the WMAP team. Assuming that they have followed similar procedures in intensity and polarization, they used a matched filter taking into account the non-Gaussian profile of the beam to detect point sources in the filtered full-sky maps, but their fluxes have been derived fitting the pixel intensities around the point source to a Gaussian profile plus a plane baseline (in the unfiltered image).

We calculated the rms noise for each patch containing an input source. This value can be easily overestimated if border effects and strong fluctuations due to other point sources or small scale structure of the diffuse emissions in the patch are not removed or filtered out. In order to avoid this, first we find the 5% brightest pixels in the patch and flag them. Second, we flag pixels within a distance equal to 15 pixels from the border (see Fig. 3). Finally, we select a shell around the source with inner radius equal to the FWHM of the beam (since polarized fluxes are never very high, this is enough for them to have decreased well below the noise level), and outer radius of $3 \times$ FWHM. The rms noise, σ, is then obtained as the square root of the variance of the pixels included in this shell, excluding flagged pixels (if any). From the distribution of the values of P in the unflagged pixels we calculate the levels exceeding those of 95.00%, 99.00%, 99.90%, and 99.99% of pixels. These are the probabilities that signals at those levels are real rather than noise
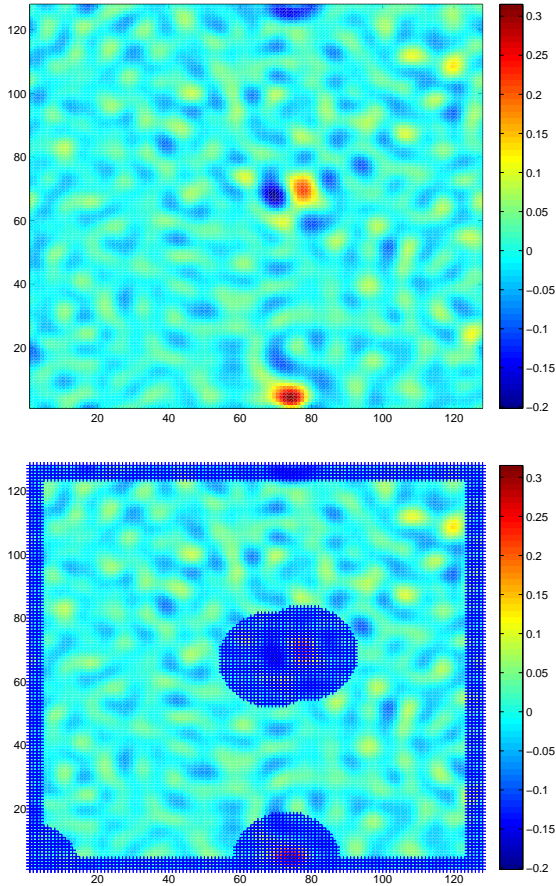
FIG. 3.— These panels show an example of the flagging of the borders and the brightest 5% objects in a given patch to prevent contaminated pixels to be used in the calculation of the background distribution. The upper panel shows a filtered patch where the bright sources are identified. The lower panel shows, cross-hatched, the flagged area.

TABLE 1
NUMBER OF DETECTIONS AT DIFFERENT SIGNIFICANCE LEVELS

Significance	23 GHz	33 GHz	41 GHz	61 GHz
95.00%	138	122	93	81
99.00%	53	41	30	20
99.90%	20	16	11	6
99.99%	18	12	9	6

fluctuations. An example is shown in Fig. 2.

3. RESULTS

In Table 1 we list the number of objects with P values significant at more than 95.00%, 99.00%, 99.90%, and 99.99% confidence levels. There are 18, 12, 9, and 6 detections with $\geq$ 99.99% significance level at 23, 33, 41, and 61 GHz, respectively. The 22 sources detected at such significance level at, at least, one frequency, are listed in Table 2. Several of them are well known bright extended objects including Cassiopeia A, Centaurus A, Cygnus A, Fornax A, Pictor A, Taurus A (Crab Nebula), and Virgo A (but, except for Cen A and For A, their sizes are smaller than the WMAP 23 GHz beam). Since our algorithm is not optimized for extended sources, the

flux estimates for these objects are likely affected by systematic errors much larger than the quoted statistical errors. In addition resolution effects can be seen in WMAP data, for example they likely account for the steep drop of the Crab polarized flux between 41 and 61 GHz. Such drop corresponds to the ratio of WMAP beam areas at these two frequencies. Five objects do not have plausible counterparts in low frequency radio surveys. They may therefore be exceptionally high peaks in the highly non-Gaussian fluctuation field, in temperature and polarization, mostly due to Galactic synchrotron (with possible CMB and source confusion contributions). In fact, 3 of these 5 objects are at $|b| < 10°$ and a fourth one (no. 346) is in the Ophiuchus Complex region.

All the 5 objects detected in polarization by Wright et al. (2009) have P values significant at $>$ 99.99% levels at least at 1 frequency. As shown by Table 3 our flux estimates are in generally good agreement with those by Wright et al. (2009), in spite of the different techniques used. The main formal discrepancy concerns the 23 GHz polarized flux of 0322-3711 (Fornax A), a well known extended source for which we expect that photometric errors are mostly systematic, as noted above.

To better assess the reliability of our estimates we have compared those sources detected at $\geq$ 95.00% confidence levels with ground based measurements at nearby frequencies. Unfortunately there are only few samples that can be used for such a comparison. The AT20G Bright Source Sample (BSS; Massardi et al. 2008) covers the declination region $\delta < -15°$ and is complete in total intensity down to $S_{20\,GHz} = 0.5\,Jy$ (except for Fornax A) and has simultaneous polarization measurements. Nine extended (i.e. with size larger than the 2.4 arcmin resolution of ATCA measurements) objects have been followed-up in polarization, mosaicing a region large enough to evaluate reasonably well the integrated polarized flux density (Burke-Spolaor et al. 2009). Despite all efforts, for some very extended objects (like Cen A) the full extent of the low-frequency radio structure could not be imaged and the total P could not be measured. Angular resolution plays a key role in the comparison of the measurements of P obtained with different instrument or configurations for extended sources. The problems are, of course, amplified if observations at different frequencies are compared: the AT20G observations showed that the polarization degree may vary with frequency. The BSS comprises 218 detections of polarized flux density, of which 19 are above 100 mJy at 20 GHz. 73 objects of our 95.00% confidence level detections are in common with the BSS, but only 28 of them have a polarization detection in the AT20G BSS, with polarized flux density typically lower than those estimated with the techniques applied here, as detailed later.

Ricci et al. (2004) have carried out 18 GHz polarization observations of the Southern portion of the Kuehr et al. (1981) sample, comprising sources with $S_{5\,GHz} = 1\,Jy$. Due to resolution effects, a source in the Centaurus A region appears with flux density larger than 1 Jy in our sample but with less than 100 mJy in the Ricci et al. (2004) sample. Variability may justify the disagreement for the blazar 3C 279 for which Ricci et al. measured $P_{18\,GHz} = 1.6\,Jy$, a factor of $\simeq 2.5$ higher than estimated from the WMAP 23GHz map.

TABLE 2
The POlarized WMAP Point Sources (POWPS) sample.

Object		RA [h]	DEC [deg]	GLON [deg]	GLAT [deg]	P (Jy) 23 GHz	P (Jy) 33 GHz	P (Jy) 41 GHz	P (Jy) 61 GHz	flags
74	(Fornax A)	3.372	-37.177	240.122	-56.766	1.07 ± 0.04	0.87 ± 0.06	0.49 ± 0.06	0.41 ± 0.10	1 1 1 4
126	(Pictor A)	5.326	-45.743	251.548	-34.680	0.38 ± 0.05	0.42 ± 0.06	0.41 ± 0.07	–	1 1 3 0
156	(PKS0607-15)	6.166	-15.679	222.609	-16.109	0.33 ± 0.04	0.36 ± 0.07	–	–	1 3 0 0
200	(PKS0829+04)	8.530	4.559	220.627	24.357	–	–	0.56 ± 0.09	1.10 ± 0.16	0 0 3 1
256	(PKS1144-37)	11.787	-38.150	289.265	23.012	–	0.49 ± 0.07	–	–	0 1 0 0
266	(NC)	12.200	-52.630	296.882	9.778	0.73 ± 0.04	0.42 ± 0.06	0.44 ± 0.07	–	1 1 1 0
272	(3C273)	12.485	2.044	289.957	64.352	1.07 ± 0.05	0.71 ± 0.06	0.72 ± 0.08	–	1 1 1 0
273/274	(Virgo A)	12.509	12.350	283.597	74.433	0.79 ± 0.05	0.71 ± 0.07	0.62 ± 0.08	0.53 ± 0.14	1 1 1 1
280	(3C279)	12.936	-5.762	305.107	57.090	0.67 ± 0.05	0.45 ± 0.08	0.83 ± 0.09	0.66 ± 0.17	1 3 1 4
289	(PKS1320-44)	13.381	-44.682	308.790	17.832	1.67 ± 0.08	1.13 ± 0.12	0.56 ± 0.13	–	1 1 3 0
291	(Centaurus A)	13.422	-43.025	309.483	19.416	3.19 ± 0.08	2.30 ± 0.11	2.02 ± 0.11	1.58 ± 0.13	1 1 1 1
295	(3C286)	13.527	30.510	56.332	80.578	0.33 ± 0.04	0.50 ± 0.06	–	0.63 ± 0.11	1 1 0 3
337	(PKS1546+02)	15.823	2.545	10.743	40.891	0.33 ± 0.05	–	–	–	1 0 0 0
346	(NC)	16.345	-25.487	351.319	17.150	0.45 ± 0.06	–	–	–	1 0 0 0
432	(NC)	20.278	45.776	82.152	5.810	1.16 ± 0.07	0.67 ± 0.07	0.38 ± 0.07	–	1 1 3 0
437	(GB6 J2038+51)	20.647	51.316	88.822	6.016	0.62 ± 0.07	0.29 ± 0.07	0.40 ± 0.07	–	1 4 3 0
439	(NC)	20.846	29.160	72.753	-9.460	0.45 ± 0.05	0.33 ± 0.06	0.31 ± 0.07	0.48 ± 0.11	1 3 4 4
440	(G93.3+6.9)	20.871	55.404	93.307	6.956	0.57 ± 0.06	0.36 ± 0.07	0.33 ± 0.06	–	1 4 4 0
473	(NC)	22.323	26.438	85.400	-25.138	–	–	–	0.95 ± 0.13	0 0 0 1
Cygnus A	(3C405)	19.984	40.484	75.930	5.700	0.49 ± 0.07	0.51 ± 0.07	0.56 ± 0.06	0.48 ± 0.12	3 2 1 4
Taurus A	(Crab)	5.583	22.369	184.310	-5.510	24.7 ± 0.18	20.2 ± 0.16	16.0 ± 0.14	6.41 ± 0.18	1 1 1 1
Cas A	(3C461)	23.408	58.835	111.872	-2.157	0.91 ± 0.05	0.55 ± 0.06	0.58 ± 0.06	0.22 ± 0.11	1 1 1 1

NOTE. — Sources detected at $> 99.99\%$ confidence level in at least one of the WMAP frequency channels. Column 1: sequential number in the NEWPS_5yr_5s catalogue and source name (NC means that the source has no plausible low radio frequency counterpart; see text); columns 2-5: equatorial (J2000) and Galactic coordinates of the source; columns 6-9: detected integrated polarized flux density and their errors at 23, 33, 41 and 61 GHz; columns 10-13: flags for significance level (1 : $\geq 99.99\%$, 2 : $\geq 99.90\%$ but $< 99.99\%$, 3 : $\geq 99.00\%$ but $< 99.90\%$, 4 : $\geq 95.00\%$ but $< 99.00\%$, 0 =< 95.00\%)$, at 23, 33, 41 and 61 GHz, respectively. The NEWPS_5yr_5s catalogue lists 2 sources (No. 273 and 274) close to the position of Virgo A. The present re-analysis has shown that they are actually the same source, coinciding with Virgo A with total flux density of 18.4 ± 0.25 at 23 GHz.

TABLE 3
Comparison of polarized flux estimates in the present paper with those of Wright et al.
(2009)

Object		$23\,GHz_{\rm W}$	$23\,GHz_{\rm p}$	$33\,GHz_{\rm W}$	$33\,GHz_{\rm p}$	$41\,GHz_{\rm W}$	$41\,GHz_{\rm p}$
0322-3711	(For A)	1.57 ± 0.07	1.07 ± 0.04	1.17 ± 0.15	0.87 ± 0.06	0.85 ± 0.23	0.49 ± 0.06
0519-4546	(Pic A)	0.39 ± 0.06	0.38 ± 0.05	0.45 ± 0.10	0.42 ± 0.06	–	0.41 ± 0.06
1229+0203	(3C273)	0.98 ± 0.06	1.07 ± 0.05	0.81 ± 0.11	0.71 ± 0.06	0.80 ± 0.13	0.72 ± 0.08
1230+1223	(Vir A)	0.75 ± 0.08	0.79 ± 0.05	0.74 ± 0.11	0.71 ± 0.07	0.50 ± 0.11	0.62 ± 0.08
1256-0547	(3C279)	0.62 ± 0.07	0.67 ± 0.05	0.55 ± 0.12	0.45 ± 0.08	0.69 ± 0.15	0.83 ± 0.09

NOTE. — The subscripts 'W' and 'p' designate the columns containing the results by Wright et al. (2009) and of the present paper, respectively.

Both the BSS and the Ricci et al. samples cover the Southern hemisphere. Among the Northern 78 VLA polarization calibrators listed in the compilation updated by S. Meyer[3] 31 are among our 95.00% significance level detections. 13 of them have polarized flux density (averaged over the epoch 2002-2006) above 100 mJy in the K band.

As mentioned above, the comparison with ground based measurements is complicated by resolution effects for the extended (generally steep-spectrum) sources and by the strong variability of the flat-spectrum ones. Nevertheless, Fig. 4 shows a reasonably good consistency for $P > 400\,\text{mJy}$ at 23 GHz. Below 400 mJy, the values of P are clearly dominated by the contribution of positive polarization fluctuations at the source positions (Eddington bias).

[3] www.aoc.nrao.edu/ smyers/calibration/master.shtml

3.1. Additional tests and simulations

Unfortunately the number of objects with polarized flux above 400 mJy and ground based polarization measurement at frequencies close to WMAP ones is small, so that our comparison has a poor statistics. To better assess the reliability of our flux estimates it is thus necessary to resort to simulations. We have selected a sample of 738 positions with $|b| > 5°$ and far from each other more than $4R_s$ (see the first paragraph of § 2.3) and more than $2R_s$ away from each object in the NEWPS_5yr_3s catalogue. These 'blank' positions (free of sources brighter than 3σ in total intensity) constitute our control fields. We have then chosen 10 values of P, ranging from 0.2 to 2 Jy, with a constant step in $\log P$, i.e. $P = [0.2, 0.26, 0.33, 0.43, 0.56, 0.719, 0.928, 1.20, 1.55, 2.0]$. For each value of P we have injected a source with that polarized flux density in the projected Q and U patches centered on 100 randomly chosen control field positions.
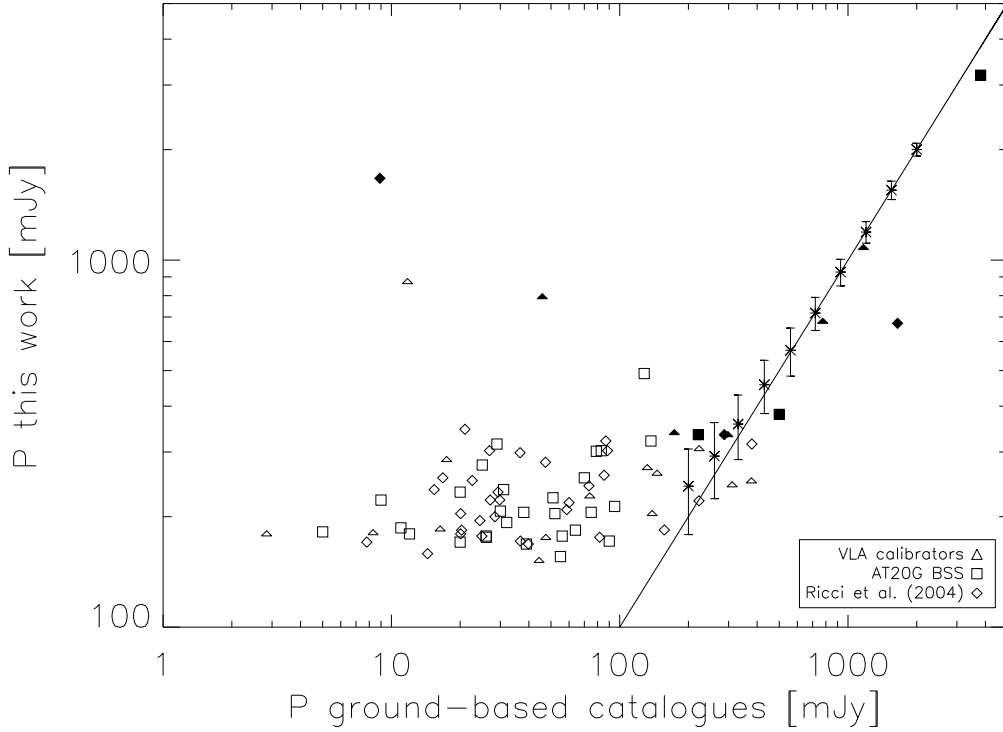
FIG. 4.— Comparison of polarized flux density estimates from the WMAP 23 GHz map (present paper) and ground-based observations: AT20G BSS (Massardi et al. 2008; squares); Ricci et al. (2004) (diamonds); VLA calibrators (triangles). Filled symbols correspond to sources detected on the WMAP map with more than 99.99% significance level. In case of sources with multiple ground-based observations, we have chosen those with the resolution closest to WMAP's. The solid line corresponds to equal values on the two axes. The two highest filled symbols on the left of the solid line are examples of the effect of the much higher resolution of ground based measurements, compared to WMAP's; the filled diamond is Cen A (resolved also by WMAP), and the filled triangle is Virgo A (unresolved by WMAP). The highest open triangle corresponds to a source close to the Galactic plane, whose polarized flux estimated from the WMAP maps includes a dominant Galactic contribution. The outlier on the right of the solid line is the highly variable blazar 3C279. The asterisks with error bars show the results of simulations described in § 3.1

This was done randomly selecting Q between $-P$ and P and setting $U = \pm\sqrt{P^2 - Q^2}$, the sign of U being again chosen at random. The inserted source was convolved with the WMAP symmetrized beam at 23 GHz. We avoided using the same patch more than once, except when all the control fields were already used. In any case the same patch was never used twice for the same value of P.

Figure 5 shows the percentage error in the values of P of the simulated sources recovered with our filtering and flux estimation process with respect to the input values. This comparison confirms the reliability of recovered fluxes for $P_{input} \gtrsim 400$ mJy, while the Eddington bias becomes increasingly important below this value. For $P_{input} = 400$ mJy the recovered fluxes are, on average, overestimated by less than 10%.

3.2. *Median Polarization Degree*

The median polarization degree at 23 GHz of the 11 sources detected with a confidence level $\geq 99.99\%$, with low radio frequency counterparts, and with $P \geq 400\,\mathrm{mJy}$ is $\simeq 7.5\%$. This value, however, is not representative of the mean polarization level of sources in a complete sample for two reasons. First, the sample is obviously biased towards sources with the highest polarization degrees.
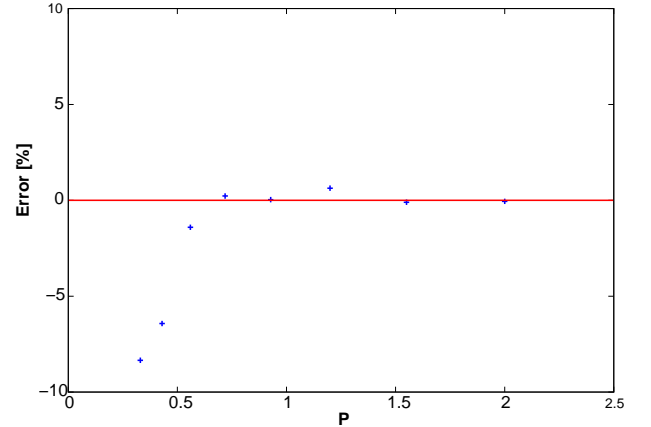

FIG. 5.— Results of the simulations for logarithmically spaced values of P in the range 0.2-2 Jy. In this panel we show the percentage error ($100(P_{input} - P_{recovered})/P_{input}$) in the recovered value of P.

Second, as mentioned above, our photometry is not optimal for extended sources which make up a substantial fraction of the sample, so that their estimated polarization degrees are highly uncertain.
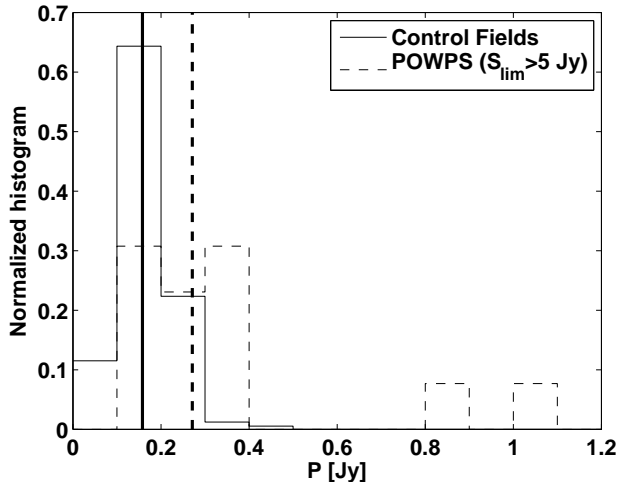
An unbiased estimate of the mean polarization degree

FIG. 6.— Distributions, normalized to unity, of P signals in the direction of the 23 GHz sources brighter than 5 Jy (13 objects; dashed histogram) compared with those for the control fields (solid). The median P values are of 0.27 Jy for sources and of 0.16 Jy for control fields. According to the Kolmogorov-Smirnov test, the probability that the two samples are drawn from the same parent distribution is of only $7.3 \cdot 10^{-5}$

of sources at WMAP frequencies can be obtained from a comparison of the distribution of P values for a suitably chosen complete subsample with that of control fields. The completeness limit, in total flux, cannot be too faint, otherwise the mean polarization level is too low to be detectable. On the other hand, if the flux limit is too high, the number of sources is too small for a meaningful statistical inference. The optimal flux limits turn out to be of 5, 4, 3, and 4 Jy at 23, 33, 41, and 61 GHz, respectively. We find a highly significant detection of polarized flux density only at 23 GHz (see Fig. 6): the probability that the distribution of P values of sources is drawn from the same parent distribution as control fields is $7.3 \cdot 10^{-5}$. The median polarization degree, Π, can be estimated as:

$$\Pi = \frac{P_{\mathrm{med,sources}} - P_{\mathrm{med,controlfields}}}{S_{\mathrm{med,sources}}}, \qquad (3)$$

where $S_{\mathrm{med,sources}}$ is the median flux of sources and we have neglected the median flux of control fields, which is close to zero. The result at 23 GHz is $\Pi_{\mathrm{23GHz}} = 1.7 \pm 1.1\%$, consistent with the median polarization degree for the AT20G BSS, $\Pi_{\mathrm{20GHz}} \simeq 2.5\%$ (Massardi et al. 2008). Note that the lower resolution of WMAP, compared to AT20G, observations make them more liable to beam depolarization (due to chaotic components of the magnetic field within the unresolved region) in the case of extended sources.

The probabilities that the distributions of P values of sources are drawn from the same parent distribution as control fields are of 0.02, 0.012, and 0.065 at 33, 41, and 61 GHz, respectively. The derived values of Π are $\Pi_{\mathrm{33GHz}} = 0.91 \pm 0.83\%$, $\Pi_{\mathrm{41GHz}} = 0.68 \pm 1.0\%$, and $\Pi_{\mathrm{61GHz}} = 1.3 \pm 1.8\%$.

3.3. *Predictions for Planck*

The Planck satellite is expected to measure the polarization of the sources with greater sensitivity than

WMAP, and therefore to detect more sources, down to fainter polarized flux limits. Building on the results of our analysis of WMAP maps, we have carried out simulations to estimate the minimum polarized flux detectable and reliably measurable by Planck. We have adopted the nominal mean instrumental noise levels expected after two complete sky surveys (1 yr)[4].

Assuming that the Q and U images are dominated by instrumental white noise, and adopting a pixel size of 6.87 arcmin and idealized matched filters for the nominal beam sizes, we have computed the ratios between the σ_P levels for the 30–100 GHz Planck frequency channels and those for the closest WMAP frequency channels. We find $\sigma_{P,\mathrm{WMAP\,5yr}}/\sigma_{P,\mathrm{Planck\,1yr}} = 2.2$, 1.6, 2.0, and 6.8 at about 30, 44, 70, and 100 GHz, respectively. Note that the higher Planck sensitivity is partly compensated by the longer WMAP exposure time. An extension of the Planck mission for one more year would decrease $\sigma_{P,\mathrm{Planck}}$ by a factor $\sqrt{2}$.

The above calculations take into account only instrumental noise. To investigate the effect also of polarization fluctuations due to diffuse foregrounds and to the CMB we have performed simulations analogous to those we did for WMAP at 23 GHz for the Planck 30 GHz channel, using the Planck Sky Model simulation software (Delabrouille et al. 2009).

In simulated Q and U maps containing polarized diffuse foregrounds and the CMB we have injected sources with P in the range 0.05–0.6 Jy. Our algorithm recovered sources with P down to 300 mJy with systematic offsets due to the Eddington bias of few percent or less.

This result already highlights the difficulty of finding suitable polarization calibrators for Planck. Not many point-like sources have P substantially larger than 300 mJy at 30 GHz. Combining the results by Ricci et al. (2004), of the AT20G BSS (Massardi et al. 2008) and the VLA calibrator observations, we have found 11 extragalactic sources above this limit. The count may be incomplete, particularly in the Northern hemisphere, but it is unlikely that many bright sources have been missed. Our analysis of 33 GHz WMAP maps, including bright Galactic sources, has detected 12 sources at a confidence level > 99.99%; polarized flux densities for most of them, however, are overestimated because of the Eddington bias. Also, some of the brightest sources are extended (compared to the Planck beam) and others (3C273 and 3C279) are highly variable.

4. CONCLUSIONS

We have applied to the WMAP 5-yr polarization maps a new source detection technique, called "filtered fusion" (Argüeso et al. 2009), taking into account the real symmetrized beam profiles. The technique was applied at the positions of WMAP sources detected at $\geq 5\sigma$ by Massardi et al. (2009), plus 3 extended sources (Cygnus A, Taurus A, Cas A) known to be bright and polarized. 22 sources were detected at a confidence level $\geq 99.99\%$ (that would correspond to $\simeq 3.72\sigma$ for a one-tailed Gaussian statistics) in at least one WMAP channel. Five of them, however, have no plausible counterparts in low radio frequency catalogs and may therefore be just high intensity peaks of the fluctuation field. Nevertheless,

this is a substantial improvement compared to the 5 source polarization measurements listed by Wright et al. (2009) and our results for these 5 sources are in generally good agreement with theirs.There are several reasons that could explain such an improvement. First, WMAP used a mask to produce the point source catalogs based on the KQ75 mask plus the Magellanic cloud regions that exclude 11 objects that we have studied. Second, WMAP did not consider objects that are not associated to known sources at low frequencies. In our case, we do a non-blind search at the positions of the NEWPS-5yr catalog that includes a handful of such objects, some of which show a significant polarized flux (marked as NC in Table 2), maybe due to Galactic emission in polarization. Taking all these into account, and considering the efficiency of our method as compared to WMAP, one could conclude that we are detecting between $30 - 40\%$ more sources, which is a similar improvement to the one obtained in our analysis in total intensity (Massardi et al. 2008).

A comparison of our polarized flux, P, estimates at 23 GHz (Fig. 4, where sources detected at $\geq 99.99\%$ confidence level are represented by filled symbols) with high signal-to-noise ground based measurements at nearby frequencies, highlights the complications due to different angular resolutions in the case of extended sources (Cen A and Vir A) and of strong variability (3C279). For sources not affected by these problems, the agreement is quite good. The latter sources, however, are too few to allow a firm conclusion on the reliability of our flux estimate. We have therefore resorted to simulations, injecting fake sources of known polarized flux density in the WMAP 23 GHz Q and U maps. The simulations showed that our approach is reliable for $P_{23\mathrm{GHz}} \geq 400$ mJy, while the Eddington bias becomes increasingly large at fainter fluxes (it is less than 10% at 400 mJy). Figure 4 also shows that estimates of P for sources detected at a confidence level $< 99.99\%$ are badly affected by the Eddington bias, and therefore unreliable. This was expected since, for example, a 99.90% confidence level corresponds to 3.1σ in the case of a Gaussian distribution of fluctuations. And, as shown by Hogg & Turner (1998), flux estimates at this confidence level are practically useless.

Analogous simulations using the mean noise levels expected after 1 year of Planck observations have shown that a few percent Eddington bias is reached for $P_{30\mathrm{GHz}} \simeq 300$ mJy. The modest difference compared to WMAP 23 GHz is due to the fact that the longer WMAP exposures (5 yrs vs. 1 yr) compensate for the lower sensitivity. In the case of an extension of the Planck mission for a second year, the gain over WMAP will increase by a factor of $\sqrt{2}$. Based on the predictions by Taylor et al. (2007; their Fig. 7), this would imply an increase of detections in polarization by a factor $\gtrsim 3$ compared to WMAP.

Sources detected on WMAP polarization maps have, on average, exceptionally high polarization degrees because only a very small fraction of sources have been detected and they likely populate the tail of the distribution of P values. Estimates of, or upper limits to, the mean polarization degrees, Π, of bright sources at 23, 33, 41, and 61 GHz have been obtained comparing the distributions of polarized flux densities in the directions of complete source samples, limited in total flux, with those in the directions of control fields, devoid of bright sources. The derived values, $\Pi_{23\mathrm{GHz}} = 1.7 \pm 1.1\%$, $\Pi_{33\mathrm{GHz}} = 0.91 \pm 0.83\%$, $\Pi_{41\mathrm{GHz}} = 0.68 \pm 1.0\%$ and $\Pi_{61\mathrm{GHz}} = 1.3 \pm 1.8\%$, are consistent with, but somewhat on the low-side of, the median polarization degree for the AT20G BSS, $\Pi_{20\mathrm{GHz}} \simeq 2.5\%$ (Massardi et al. 2008). Somewhat lower values of Π are expected at the WMAP resolution for extended sources, due to beam depolarization.

Finally, the detected sources may be candidate calibrators for other high sensitivity CMB experiments, like the ground-based QUIJOTE experiment (Rubiño-Martin et al. 2008) or the Planck satellite mission.

REFERENCES

Argüeso F., Sanz J.L., Herranz D., López-Caniego M., González-Nuevo, J., 2009, MNRAS, 395, 649
Barnard V. E., Vielva P., Pierce-Price D. P. I., Blain A. W., Barreiro R. B., Richer J. S., Qualtrough C., 2004, MNRAS, 352, 961
Bock J. et al., 2006, arXiv:astro-ph/0604101
Burke-Spolaor S., Ekers R. D., Massardi M., Murphy T., Partridge B., Ricci R., Sadler E. M., 2009, MNRAS, 395, 504
Carvalho P., Rocha G., Hobson M. P., 2009, MNRAS, 393, 681
Delabrouille J. et al., 2009, in preparation.
Eddington A. S., 1913, MNRAS, 73, 359
Feroz F., Hobson M. P., 2008, MNRAS, 384, 449
González-Nuevo J., Argüeso F., López-Caniego M., Toffolatti L., Sanz J. L., Vielva P., Herranz D., 2006, MNRAS, 369, 1603
González-Nuevo J., Massardi M., Argüeso F., Herranz D., Toffolatti L., Sanz J. L., López-Caniego M., de Zotti G., 2008, MNRAS, 384, 711

Górski K. M., Hivon E., Banday A. J., Wandelt B. D., Hansen F. K., Reinecke M., Bartelmann M., 2005, ApJ, 622, 759
Herranz D., Sanz J. L., Barreiro R. B., Martínez-González E., 2002, ApJ, 580, 610
Herranz D., López-Caniego M., Sanz J. L., González-Nuevo J., 2009, MNRAS, 394, 510
Herranz D., Sanz J. L., 2008, JSTSP, 5, 727
Hobson M. P., McLachlan C., 2003, MNRAS, 338, 765
Hogg D. W., Turner E. L., 1998, PASP, 110, 727
Homan D. C., Attridge J. M., Wardle J. F. C., 2001, ApJ, 556, 113
Kamionkowski M., Kosowsky A., Stebbins A., 1997, PhRvD, 55, 7368
Kuehr H., Witzel A., Pauliny-Toth I. I. K., Nauber U., 1981, A&AS, 45, 367
Leach S. M., et al., 2008, A&A, 491, 597

López-Caniego M., Herranz D., Barreiro R.B., Sanz J.L., 2005a, MNRAS, 359, 993

López-Caniego M., Herranz D., Sanz J. L., Barreiro R. B., 2005b, EJASP, 2005, 2426

López-Caniego M., Herranz D., González-Nuevo J., Sanz J. L., Barreiro R. B., Vielva P., Argüeso F., Toffolatti L., 2006, MNRAS, 370, 2047

López-Caniego M., González-Nuevo J., Herranz D., Massardi M., Sanz J. L., De Zotti G., Toffolatti L., Argüeso F., 2007, ApJS, 170, 108

Malik R. K., Subramanian K., 1997, A&A, 317, 318

Massardi M., et al., 2008, MNRAS, 384, 775

Massardi M., López-Caniego M., González-Nuevo J., Herranz D., de Zotti G., Sanz J. L., 2009, MNRAS, 392, 733

Nailong W., 1992, ASPC, 25, 291

Ricci R., et al., 2004, MNRAS, 354, 305

Rubiño-Martin J. A., et al., 2008, arXiv:0810.3141

Sadler E. M., Ricci R., Ekers R. D., Sault R. J., Jackson C. A., de Zotti G., 2008, MNRAS, 385, 1656

Sanz J. L., Herranz D., Martínez-Gónzalez E., 2001, ApJ, 552, 484

Sanz J. L., Herranz D., López-Caniego M., Argueso F., 2006, arXiv:astro-ph/0609351

Stewart I. M., 2006, A&A, 454, 997

Taylor A. R., et al., 2007, ApJ, 666, 201

Tegmark M., de Oliveira-Costa A., 1998, ApJ, 500, L83

Tucci M., Martínez-González E., Toffolatti L., González-Nuevo J., De Zotti G., 2004, MNRAS, 349, 1267

Tucci M., Martínez-González E., Vielva P., Delabrouille J., 2005, MNRAS, 360, 935

Vielva P., Martínez-González E., Cayón L., Diego J. M., Sanz J. L., Toffolatti L., 2001, MNRAS, 326, 181

Vielva P., Martínez-González E., Gallegos J. E., Toffolatti L., Sanz J. L., 2003, MNRAS, 344, 89

Vikhlinin A., Forman W., Jones C., Murray S., 1995, ApJ, 451, 542

Wright E. L., et al., 2009, ApJS, 180, 283